Liquid Crystals,
Vol. 37, No. 11, November 2010, 1393–1410

Taylor & Francis
Taylor & Francis Group

Fluorescent lanthanide complexes of Schiff base ligands possessing *N*-aryl moiety: influence of chain length on crossover (calamitic to discotic) phase behaviour

Nandiraju V.S. Rao[a]*, Trirup D. Choudhury[a,b], Rahul Deb[a], Manoj K. Paul[a], Thatavarthi R. Rao[c], Tuluri Francis[d] and Ivan I. Smalyukh[b]

[a]*Chemistry Department, Assam University, Silchar, India;* [b]*Physics Department, University of Colorado at Boulder, Boulder, CO, USA;* [c]*Chemistry Department, Banaras Hindu University, Varanasi, India;* [d]*Physics Department, Jackson State University, Jackson, MS, USA*

(*Received 17 August 2010; final version received 17 August 2010*)

New lanthanide complexes, Tb(III), Dy(III) and Gd(III) of *N*-aryl based Schiff bases exhibiting mesomorphism have been synthesised and characterised. The crossover phenomena of calamitic lamellar to discotic columnar phase behaviour in these lanthanidomesogens is found to be controlled by the variation in chain length of the single alkyl substituent on the terminal *N*-aryl ring, hitherto the first case of a metallomesogen with only one alkyl chain length at each end of the ligand as evidenced by thermal microscopy studies and complemented by X-ray studies. It is also observed as a function of temperature in a single component. The electronic properties of these systems are dominated by the donor–acceptor substituted organic chromophore ligand, and the emission maxima revealed a large Stokes shift of 160 nm. The ligand–ligand charge transfer is reflected in emission spectra and is due to the presence of phenyl rings in the ligands.

Keywords: lanthanide complexes; lanthanidomesogen; Schiff bases; crossover phase behaviour; metallomesogens; liquid crystal

1. Introduction

Metal-containing liquid crystals called metallomesogens have received a lot of attention in the past few decades due to their importance in basic liquid crystals research as well as their potential utility in industrial, chemical, medical and sensor applications [1–17].

The nature of metal plays an important role to influence the liquid crystalline properties of the material in which it is coordinated [1–17]. However, mesogenic as well as non-mesogenic ligands exhibit liquid crystalline behaviour when coordinated with a metal ion. The majority of the metallomesogens that have been studied up to now consist of d-block elements namely Cu(II), Ni(II), VO(IV), Pd(II) and Pt(II) [10, 11]. However the studies related to coordination of f-block elements, in particular the trivalent lanthanide or actinide ions with ligands exhibiting liquid crystalline behaviour, are meagre [12–36]. The first calamitic bidentate salicylideneimine, $nO(OH)m_{ali}$, possessing *N*-aliphatic moiety based lanthanide complexes (lanthanidomesogens) [14] was reported in 1991 by Galyametdinov and coworkers. However, efforts to coordinate f-block metals with the salicylideneimine-based ligands with an aryl moiety [12, 20–38] on the nitrogen atom of the central bridging imine group have been unsuccessful.

Similarly attempts at complexation of the lanthanide ions with *N*,*N*′-aromatic donors [38] (Figure 1), namely 4,7-disubstituted phenanthroline (**L1** and **L2**), or 4,4′-dimethoxy-2,2′-bipyridine (**L3**) were successful, while those with diethyl-2,2′-bipyridine-4,4′-dicarboxylate (**L4**) were unfruitful and yielded the unreacted ligand. The latter has been accounted for by an electronic destabilisation of the ester groups on the aromatic bipyridine core, associated with a more flexible conformation with respect to the phenanthroline to make this ligand not compatible for chelation with a lanthanide ion of any size. In fact the influence of the substituents on the basicity and the coordination ability of the *N*,*N*′-aromatic ligands, namely 4,4′-dimethoxy-2,2′-bipyridine (**L3**), the bipyridine bearing a methoxy group in 4,4′ positions, produced high yields of the complexes, reflecting the dramatically enhanced activation towards coordination. However, modification of the phenanthroline ligand (**L5**) in 5,6-positions fused with a substituted imidazo ring led the realisation of the nematic phase [39].

Earlier attempts to generate mesomorphic lanthanide complexes, namely lanthanidomesogens of aromatic tridentate binding units [40–43], had failed due to the bent shape of tridentate aromatic core which does not match the classical molecular geometrical criteria required for calamitic (rod-like) and columnar (disc-like) mesomorphism. However, modification [19, 43–46] in the interfacial curvature between the aromatic core and aliphatic region by an increase

*Corresponding author. Email: drnvsrao@gmail.com

ISSN 0267-8292 print/ISSN 1366-5855 online

DOI: 10.1080/02678292.2010.517328
http://www.informaworld.com

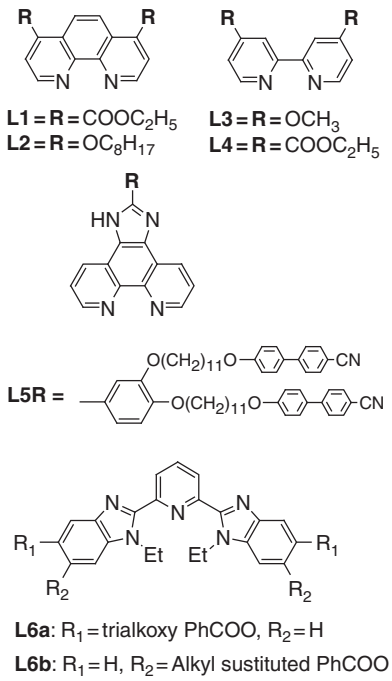

Figure 1. Molecular structure of *N*, *N*′-aromatic donors for complexation.

in the volume fraction of the alkyl chains of the tridentate aromatic (**L6a**) core promoted mesomorphic behaviour, while mesomorphism was not realised in complexes of ligand **L6b**.

Benzylideneanilines, possessing an imine double bond, are good polarisable systems. The introduction of an *ortho* hydroxyl group to the imine linkage in the benzylidene moiety not only stabilises the molecule due to intermolecular hydrogen-bonding resulting in a more planar molecule, but also promotes chelation abilities with d-block and f-block metal ions. Even though the complexation of *N*-substituted alkylsalicylideneimines, **L7–L10** (Figure 2) with lanthanide elements was successful, efforts to coordinate f-block metals with the salicylideneimine-based ligands with an aryl moiety on the nitrogen atom of the central bridging imine group were unsuccessful. Hence any attempt at the coordination of metals of the lanthanide group with any of the ligands possessing an aryl moiety on the nitrogen atom presents a special experimental challenge [47, 48].

Thus, complexation of a metal ion of high coordination number with a promesogenic ligand to exhibit mesomorphism is one of the great attractions. Since lanthanide (III) ions have many unique properties such as high coordination number (8–9), strong luminescence, magnetic behaviour, etc., we attempted to experiment with the synthesis of lanthanide complexes with Schiff base ligands, **L11–L13** (Figure 3), possessing an aromatic moiety on the

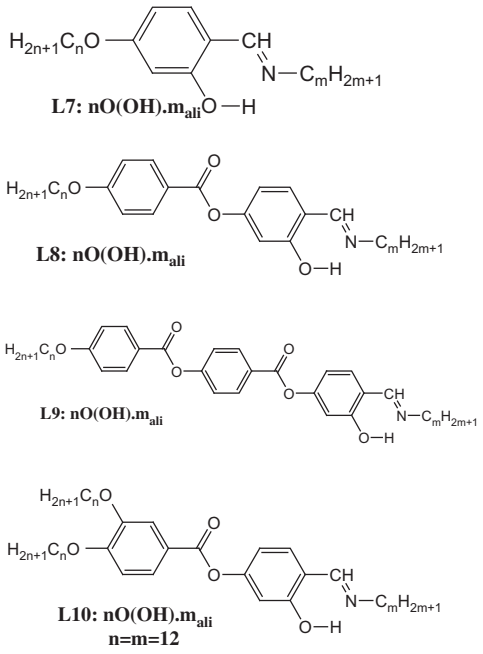

Figure 2. Molecular structure of Schiff's base ligands studied extensively for complexation [12, 24–33, 41, 42, 48].

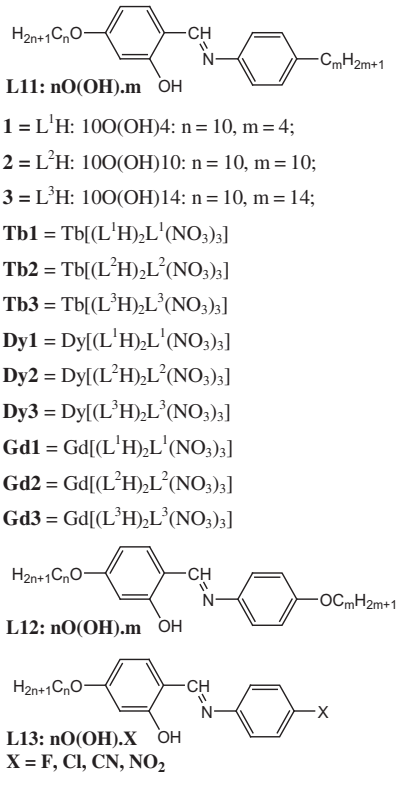

Figure 3. Molecular structures of the compounds studied in the present work.

nitrogen atom, which may promote new molecular structures with possible extension of the molecular length with aryl or aliphatic moieties and different substituents. Our previous attempts had been successful in reporting the complexation of terbium and dysprosium with *N*-(4-n-heptyloxysalicylidene)-4′-n-tetradecylaniline [7O(OH)14] [49].

In continuation of earlier work we report here the complexation of different lanthanide(III) ions with *n*O(OH).*m* **L11**, compounds with changes in the molecular length of aliphatic moieties in the *N*-aryl moiety and characterisation of mesomorphism of the complexes. The compounds studied are 10O(OH).4 (L^1H = 1), 10O(OH).10 (L^2H = 2), 10O(OH).14 (L^3H = 3) and their complexes of terbium (Tb1, Tb2, Tb3), dysprosium (Dy1, Dy2, Dy3) and gadolinium (Gd1, Gd2, Gd3).

2. Experimental details

All the chemicals were procured from M/s Frinton Laboratories, Alfa Aesar, Tokyo Kasei Kogyo Co. Ltd. The solvents and reagents are of AR grade, and were distilled and dried before use. The synthesis of ligands, namely *N*-(4-n-decyloxysalicylidene)-4′-n-alkylanilines and their lanthanide complexes, was carried out following the procedure described in Scheme 1.

Microanalysis of C, H and N elements were determined on a Carlo-Erba 1106 elemental analyser. IR spectra were recorded on a Perkin-Elmer L 120-000A spectrometer (ν_{max} in cm^{-1}) in KBr pellets. The ^1H NMR spectra of all the organic ligands were recorded in $CDCl_3$ solution on a JEOL AL300 FTNMR spectrometer. Chemical shifts are reported in parts per million (δ) relative to tetramethylsilane (TMS) as internal standard. The phase transition temperatures and associated enthalpies were recorded using differential scanning calorimetry (DSC) (Perkin-Elmer Pyris-1 system). The liquid crystalline properties of the different phases exhibited by the ligands and complexes were observed and characterised using a polarising microscope (Nikon optiphot-2-pol attached with hot and cold stage HCS302, with STC200 temperature controller configured for HCS302 from INSTEC Inc. USA). The X-ray diffraction analyses were carried out using an unoriented sample contained in 1 mm diameter quartz capillary tubes and data were collected using a point detector mounted on a Huber four-circle goniometer at Cu K(α) radiation from a Rigaku UltraX-18 rotating anode generator. UV visible absorption spectra of the compounds in $CHCl_3$ at different concentrations were recorded on a Shimadzu UV-1601PC spectrophotometer (λ_{max} in nm). Fluorescence spectra were recorded with a Shimadju RF-5301PC spectrofluorimeter with a 150W xenon lamp as the excitation source.

3. Results and discussion

3.1 Synthesis and characterisation

The synthetic procedure for ligands *N*-(4-n-decyloxysalicylidene)-4′-n-butylaniline, (hereafter abbreviated 3-*n*-*m*, 3-10-4, n = 10, m = 4, L^1H = 1, where n and m indicate the number of carbon atoms in alkyl chains), *N*-(4-n-decyloxysalicylidene)-4′-n-decylaniline, (3-10-10, L^2H = 2) and *N*-(4-n-decyloxysalicylidene)-4′-n-tetradecylaniline, (3-10-14, L^3H = 3) is presented in Scheme 1. The Schiff bases

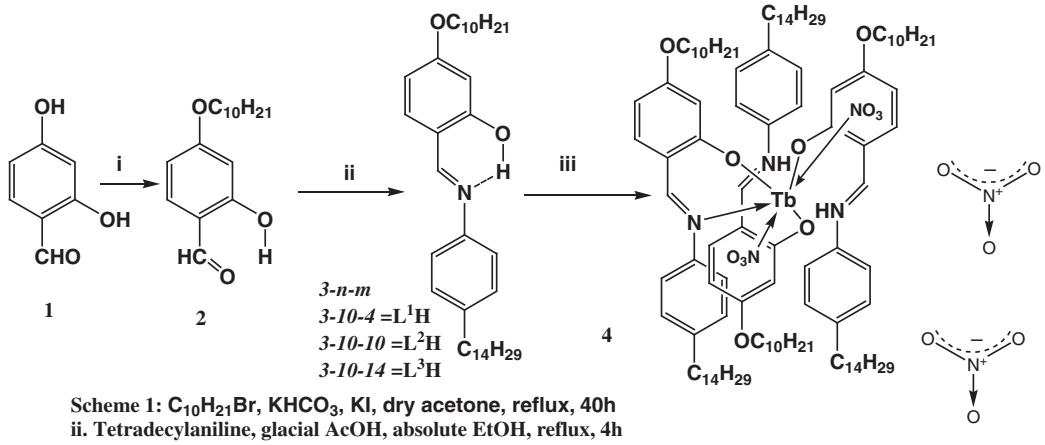

Scheme 1: $C_{10}H_{21}Br$, $KHCO_3$, KI, dry acetone, reflux, 40h
ii. Tetradecylaniline, glacial AcOH, absolute EtOH, reflux, 4h
iii. $Tb(NO_3)_3$; Acetonitrile/ EtOH, reflux, 4h
For the sake of clarity the coordination of oxygen atoms of nitrate ion is shown through nitrate ions.

Scheme 1. Synthesis of the compounds.

were synthesised using appropriate aniline following well-documented literature procedures [50] with minor modifications and were identified by ^{1}H NMR and elemental analysis (Table 1). The freshly prepared metal nitrates $Tb(NO_3)_3.6H_2O$, $Dy(NO_3)_3.6H_2O$ and $Gd(NO_3)_3.6H_2O$, from the respective metal carbonates in excess, were reacted with the ligands L^1H **(1)**, L^2H **(2)**, L^3H **(3)** in absolute ethanol or acetonitrile to yield the relevant lanthanide complexes. The synthesis of the ligands and complexes is outlined in Scheme 1.

The exact stoichiometry of these mesogenic complexes is found to be difficult due to the relatively large molecular weight of the complexes. The earlier reports also inferred that the stoichiometry depends on the nature of the ligand, as well as to a certain extent, metal ion and counter ion. Even though there was discrepancy about the stoichiometry in the literature [19–37] namely $La(LH)_3(X)_3$ [19–28] or $La(LH)_2L(X)_2$, [28–37], our experimental data confirmed the composition of the present complex as $[Ln(LH)_2L(NO_3)_2]$ (where Ln = Tb, Dy and Gd) based on the elemental analysis (Table 1), mass spectra and infrared (IR) study.

Table 1. Elemental analysis of the ligands and complexes.

Compound	%C	%H	%N
1	79.02 (79.17)	9.52 (9.60)	3.41 (3.42)
2	80.39 (80.27)	10.29 (10.41)	2.89 (2.84)
3	80.91 (80.82)	10.69 (10.82)	2.49 (2.55)
Tb1	63.72 (64.40)	7.31 (7.74)	4.56 (4.64)
Dy1	63.03 (64.24)	7.37 (7.72)	4.45 (4.62)
Gd1	61.37 (64.47)	7.52 (7.75)	4.49 (4.64)
Tb2	66.33 (67.44)	8.21 (8.69)	4.01 (3.97)
Dy2	65.51 (67.44)	8.20 (8.69)	3.95 (3.97)
Gd2	67.00 (67.50)	8.29 (8.70)	3.89 (3.98)
Tb3	66.29 (69.02)	8.23 (9.18)	3.49 (3.63)
Dy3	66.68 (68.89)	8.23 (9.17)	3.58 (3.62)
Gd3	66.75 (69.08)	10.09 (9.19)	3.54 (3.63)

Note: Values in parentheses represent theoretical values.

The metal ligand composition in the complexes is 1:3 where one Schiff base ligand of the three ligands exists in ionic form and is bonded to the metal ion in bidentate fashion, while the other two ligands exist in zwitterionic form. Hence the zwitterion is coordinated in a monodentate fashion through an oxygen atom only, while the nitrogen atom becomes protonated to bear positive charge. The negatively charged phenolic oxygen atom can readily participate in coordination with metal ions, which can also be rationalised by the tendency of lanthanide ions to preferentially coordinate with negatively charged ligands; this is supported by a shift to lower wave number in IR absorption (Figure 4).

The presence of two nitrate ions in the complex is inferred from the elemental analysis. However, the discrepancy observed between the theoretical and experimental values in elemental analysis may be attributed to the association of solvent molecules. Further time-of-flight (TOF) mass spectra of Tb2 (Figure 5(a)) and Gd3 (Figure 5(b)) reflected the

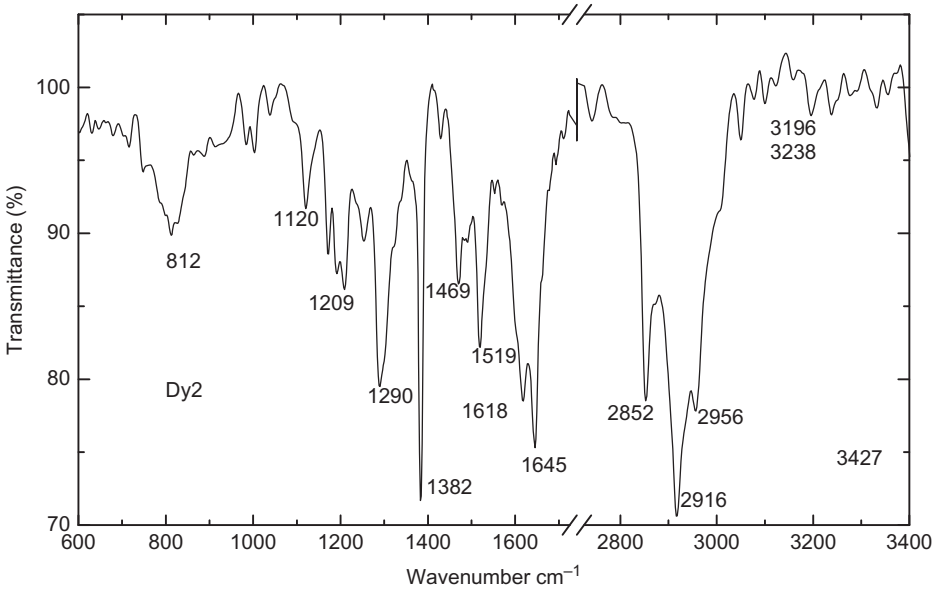

Figure 4. Representative FTIR spectrum of Dy2.

presence of two nitrate ions coordinated with the metal in the complex. These two nitrate ions depart as a neutral HNO_3 molecule (each unit has a molecular weight of 63), taking two protons from two zwitterionic ligands during fragmentation and leaving the most stable fragment as $[LnL_3]$ where all the three ligands are coordinated to metal in bidentate fashion.

The molecular structure by single crystal X-ray studies in the solid state [21] also revealed that the phenolic protons of two of the three ligands

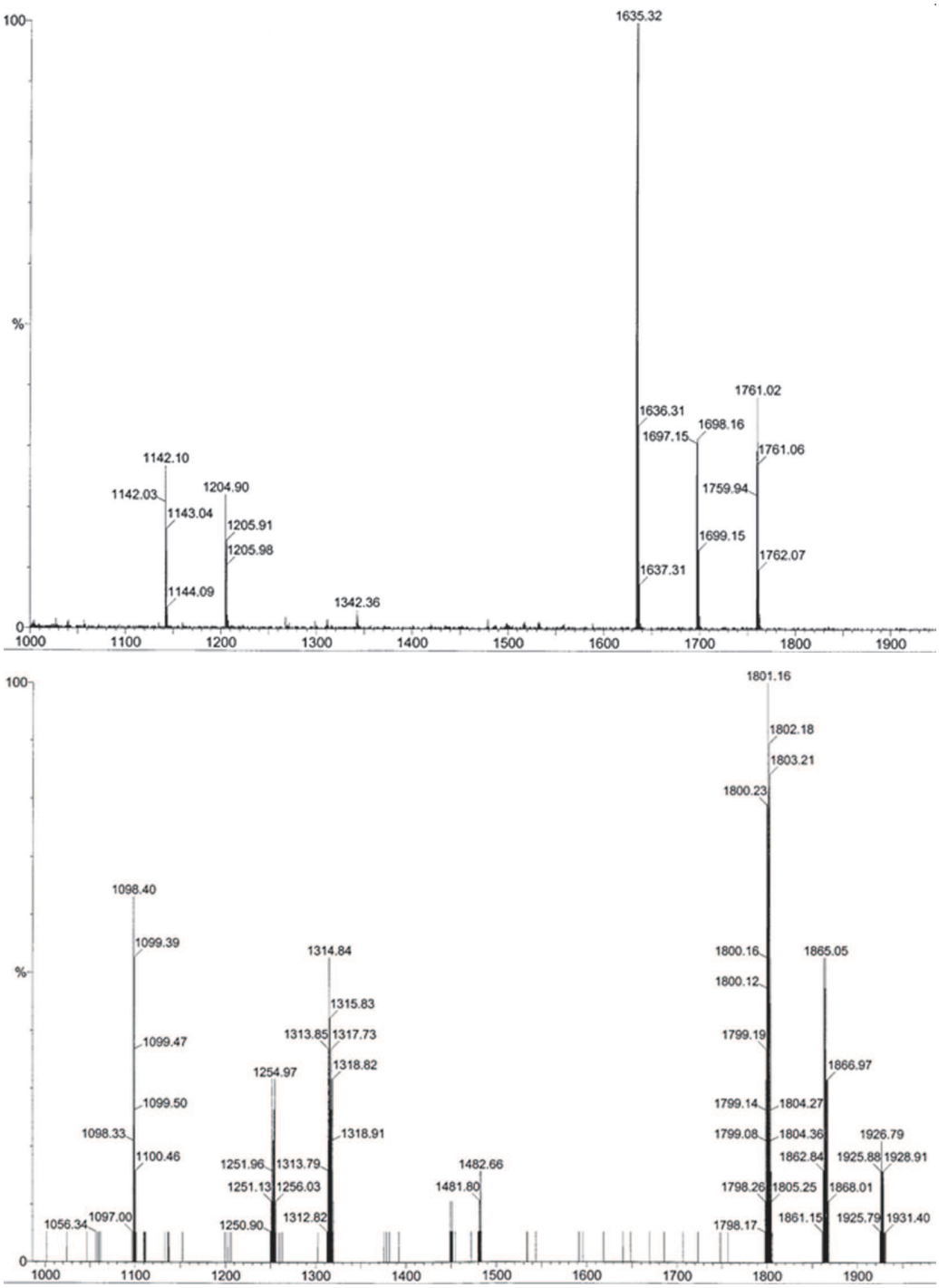

Figure 5. (a) TOF mass spectrum of Tb2; (b) TOF mass spectrum of Gd3.

transferred from oxygen to nitrogen atom not only form hydrogen bonds with the phenolic oxygen but also participate in bonding with the oxygen atoms of nitrate groups. The third ligand is present in bidentate form as evidenced by the observed band at 1616 cm^{-1} in the IR spectrum, suggesting the coordination number as eight.

The IR data also support a similar type of behaviour in these complexes. We assume that the shape of the molecule is hollow cylindrical or trigonal prismatic [29], in which the central lanthanide ion is present on the cylindrical axis with the two nitrate ions located above and below the metal ion.

3.2 Infrared spectra

The room temperature IR spectra exhibited characteristic bands [ν(C = N)] at 1629 or 1623 cm^{-1} for the ligands, and 1644 ± 1 cm^{-1} and 1616–1622 cm^{-1} for the complexes (representative IR spectrum of the complex Dy2 are presented in Figure 4), apart from the characteristic bands of the aromatic ring (C = C), Ar(C–H), CH_3 and CH_2 vibrations as listed in Table 2. The weak O–H stretching vibration of the ligand at 2870–2850 cm^{-1} overlapped by the CH modes is shifted as a broad band at 3200 ± 10 cm^{-1} in the lanthanide complexes, reflecting the N–H vibration of the protonated nitrogen atom in $C=N^{+}H$ as well as the participation of the hydrogen atom in the intramolecular hydrogen bonding with the phenolic oxygen atom as evidenced by the broadness of the peak. This abnormal behaviour may be due to coordination of the metal through the oxygen atom of the ligand only (the proton of the oxygen atom migrates to the nitrogen atom of the imine moiety), which may lead to formation of the zwitterion ($C=N^{+}$–H) of the ligand.

The observed vibrations of two bands at 1645 cm^{-1} and 1616 cm^{-1} for the complex, $Tb[(L^2H)_2(L)].(NO_3)_2$, are due to two types of CH = N stretching and compression vibrations. One of these is the elongated stretching, namely exactly opposite an increase in the imine C = N stretching vibration by 25 cm^{-1} of the complex (at 1645 cm^{-1}) in the IR spectrum compared with the stretching vibration in the free Schiff base ligand, while the other one is a compressed imine bond appearing at a lower value of 1616 cm^{-1}.

The vibration at the higher frequency (1645 cm^{-1}) is due to the complexation of the oxygen atom with the rare earth ion. This is exactly opposite to the observation of the imine C = N stretching vibration of the Cu(II) complex of L^1H [$Cu(L^1)_2$ at 1607 cm^{-1}] in the IR spectrum, which is lower than the imine C = N stretching vibration of the free ligand L^1H (1623 cm^{-1}), indicating a decrease in strength of the double bond character of C = N bond. Hence the lower value of 1616 cm^{-1} clearly indicated a similar type of coordination of the complexation as in copper complexes which take place through the deprotonated phenolic oxygen and azomethine nitrogen atoms.

The phenolic C–O stretching vibration, which is observed in the Schiff base ligands around 1290 cm^{-1}, overlaps in the metal complexes with a vibration due

Table 2. IR data of the ligands and complexes.

Compounds	ν O–H	ν N^{+}–H	ν_{as} CH_3 ν_{as} CH_2	ν_{s} CH_3 ν_{s} CH_2	ν C = N	ν (C = C)ar	ν C–O
1	2850		2956 2921	2873 2850	1629	1599 1479	1298
Tb1		3210	2956 2924	a 2854	1643 1622	1518 1476	1290
Gd1		3210	a 2918	a 2849	1642 1620	1519 1472	1289
2	2850		2955 2917	2872 2850	1623	1599 1470	1285
Tb2		3200	2954 2922	a 2853	1644 1616	1519 1474	1290
Dy2		3196	2956 2916	– 2852	1645 1618	1519 1469	1290
Gd2		3210	a 2918	a 2848	1642 1621	1519 1471	1290
3	2850		2956 2922	2872 2850	1622	1599 1478	1290
Tb3		3190	a 2918	a 2849	1643 1618	1519, 1465	1288
Dy3		3189	a 2918	a 2849	1643 1618	1518, 1468	1290

Note: a Appeared as an overlapped band or as a shoulder.

to the nitrate groups. The four bands of the coordinated nitrate group reflecting the vibrations of ν_4, ν_1, ν_2 and ν_6 are observed in the IR spectrum of Dy2 at 1468, 1289, 1121 and 841 cm^{-1}, respectively. Even though it may be assumed that monodentate nitrate group participates in coordination, the large difference in the peak positions of the bands of ν_4 and ν_1 (179 cm^{-1}) characterises the coordination of a bidentate nitrate group rather than a monodentate nitrate group.

3.3 Thermal behaviour: DSC and thermal microscopy

3.3.1 Ligands

All the three Schiff bases (i.e. salicylideneimine ligands) exhibit liquid crystalline behaviour. The liquid crystalline phases were identified by the observed optical textures using a polarised microscope attached with a hot stage. The thermodynamic data of all the compounds are presented in Table 3; the phase transition temperatures obtained from DSC and thermal microscopy are found to be in good agreement with each other. All thermal data presented in this table correspond to the first heating cycle in DSC because no transition peak was observed in the second heating for the complexes due to their decomposition in the DSC chamber. Compound **1** exhibits nematic (two-fold and four-fold brush schlieren and marble textures) and smectic C (SmC) (four-fold brush schlieren texture) phases. Compounds **2** and **3** exhibit SmC and smectic F (SmF) (chequer-board broken focal conic fan texture [51, 52]) phases, and both these compounds crystallised below room temperature. The SmC and SmF phases are confirmed by miscibility studies with known standard samples.

Preliminary results on L12 ($m = n = 10$) and L13 ($n = 16$, X = F) revealed that both the ligands exhibit mesomorphism. The synthesis of lanthanide complexes of both the ligands (in particular *N*-aryl ligand, L13, with an electron-withdrawing group substituent) was also successful. Further studies of these compounds are in progress.

3.3.2 Complexes

In the studies of thermal polarised light microscopy, a thin film of the terbium complex **Tb1** melted at 167.5°C (165.3°C by DSC) to form a highly viscous phase which cleared to isotropic fluid at 181.5°C (181.3°C by DSC) in the heating cycle. This transition enthalpy reflects a crystal-to-crystal transition. On cooling it exhibited a monotropic smectic A (SmA) phase at 178.5°C (150.3°C, 3.02 kJ/mol) with characteristic batonnets and focal conic fan shaped textures (Figure 6). This phase was further transformed to a columnar phase and finally crystallised, complementing the observation of two peaks shown in DSC during the cooling cycle at 144.6°C (1.28 kJ/mol) and 139.8°C (1.38 kJ/mol). Even though the transformation from the SmA phase to the columnar (SmA 144.6° Col_h in the cooling cycle) can be reliably detected by DSC with a decreased value of enthalpy of transition in comparison to the enthalpy in the heating cycle, the transition temperatures and the phase ranges did not match. However, the observed discrepancy between the thermal behaviour monitored by optical microscopy and DSC transition temperatures in the cooling cycle may be due to thin film used in microscopy and the highly viscous nature of bulk sampling negating the equilibrium conditions to reflect the supercooling in DSC. The supercooled glassy liquid crystalline phase texture could still be observed at room temperature. The X-ray studies also supported the observation of columnar phase at lower temperature (discussed later).

On cooling, the sample **Tb2** exhibited batonnets with homeotropic regions which coalesced to give the focal conic fan texture of SmA at 181.5°C. Furthermore, on slow cooling at 0.2°C min^{-1}, slow transformation in the texture was observed at 157.5°C which resembled a columnar texture and was different from the normal fan-like textures of SmA phase. The sample did not crystallise and the texture was retained until room temperature as a paramorphotic texture of a glassy phase. The observed textures are presented in Figure 7.

The enthalpies as observed from the DSC spectrum of **Tb2** (Figure 8) in heating cycle are much higher than the recorded enthalpies in cooling cycle. The low values of the enthalpies and the temperature range of the phase transitions indicated the nature of the sample as highly viscous possessing ordered phases. Orientational freezing always accompanied by positional ordering in the formation of smectic/columnar phases may be the plausible reason for such lowered enthalpy of transitions. **Tb3** on slow cooling from an isotropic phase sample at 0.2°C min^{-1} exhibited a uniform birefringent fan-like texture predominantly distributed in the entire region, with two brush defects at 190.1°C resembling a typical hexagonal columnar mesophase. This was followed by another transition at 82.2°C with transition bars like striated arcs across the fans, indicating an ordered smectic phase, which persisted until room temperature and was in agreement with the transition temperatures observed in DSC and X-ray studies.

The sample did not crystallise and the texture was retained until room temperature as a paramorphotic texture resembling a glassy phase (Figure 9). Dysprosium complex Dy1 exhibited crystal-to-crystal transitions in the heating cycle as evidenced by DSC

Table 3. Mesomorphic phase transition temperatures (T °C), associated enthalpies (ΔH) and entropies (ΔS) of the phase transitions of *N*-(4-n-alkyloxysalicylidene)-4′-n-tetradecylanilines and lanthanide complexes of *N*-(4-n-alkyloxysalicylidene)-4′-n-tetradecylanilines.

Compound	Transition	T (°C)	ΔH (kJ.mol^{-1})	ΔS (J.mol^{-1}.K^{-1})
1	K–SmC	45.3	22.1	69.4
	SmC–N	75.8	0.29	0.8
	N–I	87.9	1.50	4.1
	I–N	87.0	1.50	4.1
	N–SmC	74.8	0.48	1.3
	SmC–K	< 30	–	–
2	K– SmC	53.4	44.5	136.3
	SmC– I	101.8	8.4	22.5
	I– SmC	100.7	8.1	21.8
	SmC–SmF	68.1[tm]	—	—
	SmF–K	< 30	—	—
3	K–SmF	61.6	40.0	119.6
	SmF–SmC	62.7	1.42	4.2
	SmC–I	100.2	10.6	28.4
	I–SmC	99.6	10.6	28.4
	SmC–SmF	51.0	0.86	2.6
	SmF–K	34.2	14.3	46.5
Tb1	K1–K	165.3	24.8	56.7
	K– I	181.3	41.4	91.2
	I–SmA	150.3	3.0	7.1
	SmA–Col_h	144.6	1.2	3.0
	Col_h–K	139.8	1.3	3.3
Tb2	K– Col_h	150.2	20.5	48.5
	Col_h–SmA	160.8	7.7	17.9
	SmA–I	183.7	17.3	37.9
	I–SmA	178.6	2.2	5.0
	SmA–Col_h	158.1	0.20	0.4
	Col_h–K	154.9	1.4	3.2
Tb3	K1– K	62.6	18.2	54.4
	K– Sm2	84.7	48.6	136.0
	Sm2–Col_h	143.7	8.2	19.8
	Col_h–I	188.5	1.7	3.8
	I– Col_h	187.5	2.8	6.1
	Col_h– K	a		
Dy1	K–1–K	161.6	33.2	76.5
	K– I	179.3	45.0	99.6
	I–SmA	144.1	18.6	44.6
	SmA–K	a	–	–
Dy2	K–SmA	158.3	43.9	101.9
	SmA–I	177.0	12.2	27.1
	I–SmA	160.2	0.8	1.9
	SmA–Col_h	143.1	0.3	0.7
	Col_h–K	a		
Dy3	K1–K	62.9	9.36	27.8
	K–Col_h	91.9	47.3	129.8
	Col_h–SmA	141.1	4.11	9.9
	SmA–I	198.2	3.68	15.1
	I–SmA	191.5	3.63	15.1
	SmA–Col_h	a	–	–
Gd1	K–I	173.2	56.8	127.3
	I–K	128.1	3.41	8.5
Gd2	K–SmE	52.8	14.2	43.8
	SmE–SmA	99.1	1.65	4.44
	SmA–I	163.7	17.4	39.9
	I–SmA	161.0	0.19	0.45
	SmA–SmE	113.5	13.5	34.9
	SmE–K	a		
Gd3	K–SmE	62.0	57.8	172.5
	SmE–SmA	99.6	10.4	28.0
	SmA–I	151.1	34.8	82.1
	I–SmA	110.0	24.3	63.4
	SmA–SmE	88.6	3.0	8.4
	SmE–K	a		–

Notes: a Supercooled phase until room temperature. Col_h = hexagonal columnar phase. K and K1 = crystal phase. N = nematic. Sm A = Smectic A. Sm C = Smectic C. Sm E = Smectic E. Sm F = Smectic F.

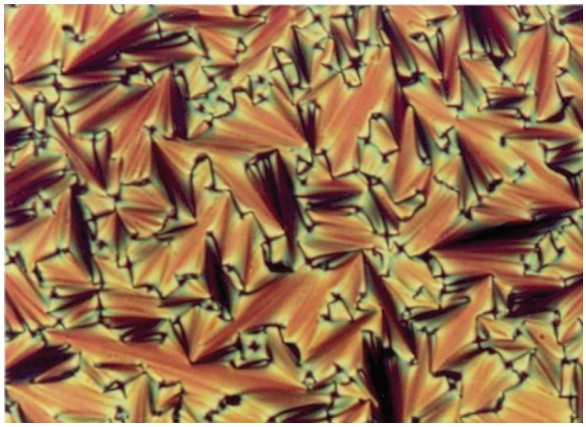

Figure 6. Focal conic structure of SmA of Tb1 at 149°C (colour version online).

and monotropic SmA phase (Figure 10(a)) in the cooling cycle. Dy2 and Dy3 exhibited SmA and columnar phases (Figure 10(b), (c)). No liquid crystalline phase was detected in gadolinium complex Gd1 even after repeated heating and cooling under the microscope; this may be due to the highly viscous nature of the compound (also supported by DSC). However, Gd2 (Figure 11) and Gd3 exhibited SmA and smectic E (SmE) phases as evidenced by the optical textures.

The gradual decrease in the radius of the lanthanide ion over the lanthanide series (lanthanide contraction), without any change in charge, contributes to stronger electrostatic attractions between the lanthanide ion and the coordinating moieties; thereby increasing the melting point of complexes in ascending order of atomic number of lanthanum ion. The rapid increase in the melting points of Gd2-Tb2-Dy2 and Gd3-Tb3-Dy3 homologues reflects this phenomenon. We did not observe the same trend in the Gd1-Tb1-Dy1 series. The increase in clearing temperatures as well as in the mesomorphic range was also observed in the Gd3-Tb3-Dy3 series. With the limited data available, however, it is difficult to explain why such a phenomenon is not observed in other series.

A crossover phenomenon from SmA to columnar phases is reflected in the microphotographs of temperature-controlled optical microscopic studies (Figure 7) – also evidenced by X-ray studies as discussed in the next section. Elliot *et al.* [53, 54] reported a changeover from a lamellar to a hexagonal columnar disordered phase as a function

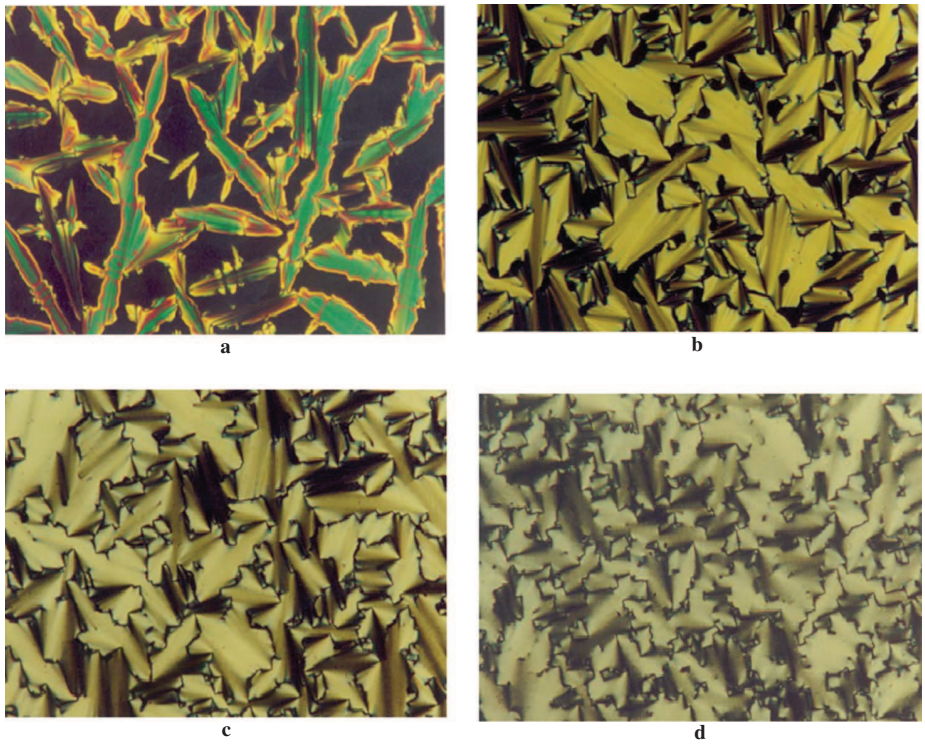

Figure 7. Textures exhibited by Tb2 in SmA and columnar phases: (a) batonnets and homeotropic texture of Tb2 at $T = 170$°C; (b) columnar texture of Tb2 at $T = 158$°C; (c) columnar texture of Tb2 at $T = 110$°C; and (d) paramorphotic columnar texture of Tb2 at $T = 35$°C (colour version online).

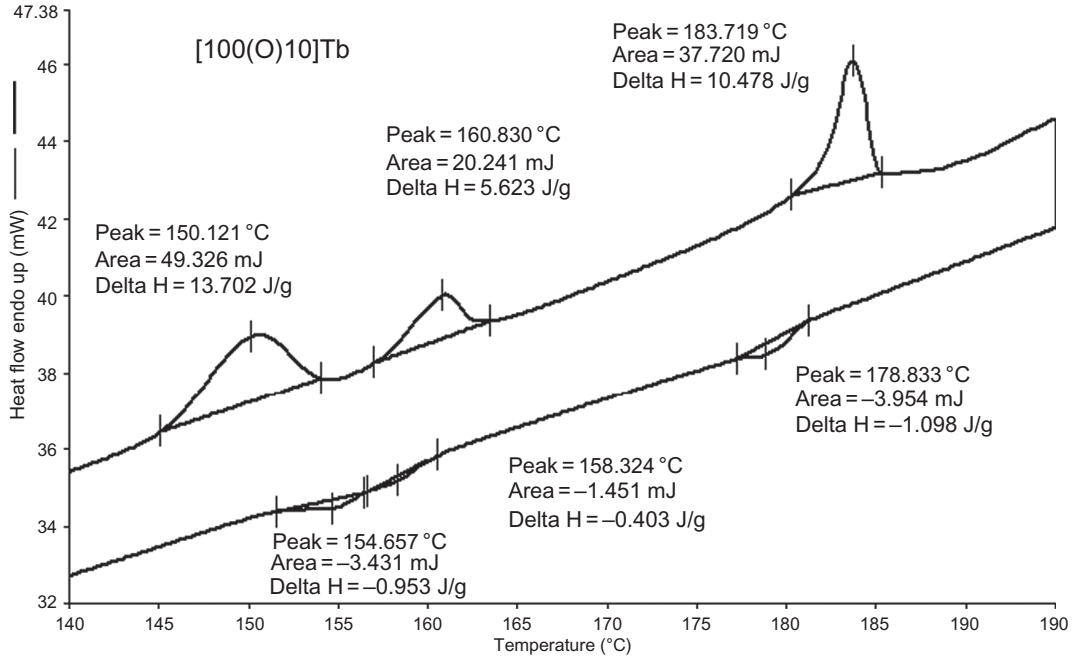

Figure 8. DSC spectrum of Tb2.

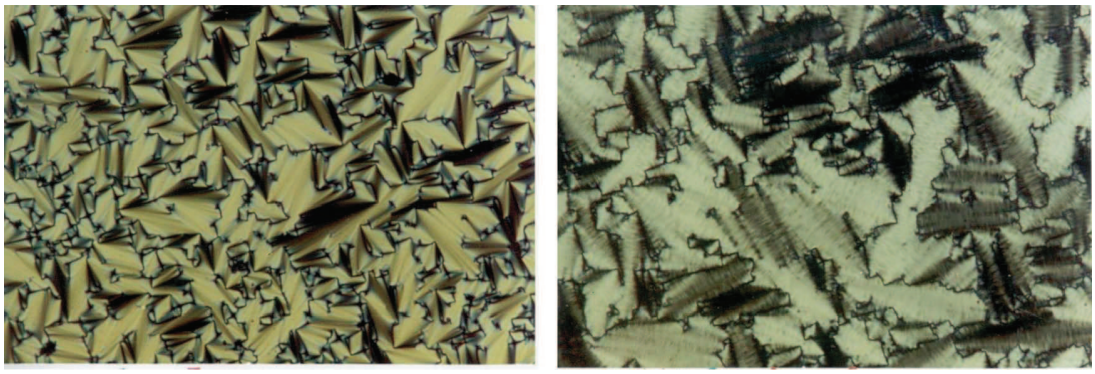

T = 180 °C T = 40 °C

Figure 9. Columnar and striated arc textures exhibited by Tb3 at different temperatures (colour version online).

of chain length in a homologous series in polycatenar systems of bis[5-(3,4-dialkoxybenzylidene)-aminotropolonatocopper(II) when the alkyl chain length is increased to the tridecyl homologue.

A similar observation of hexagonal columnar phases is also reported in lanthanide complexes of *N*-dodecyl-4-(3′,4′-didodecyloxy- benzoyloxy)salicylideneimine possessing polycatenar alkyloxy chains [32, 55]. Dependent on the number of chains, a discontinuous transition from a lamellar to a columnar organisation is observed [56] in mononuclear *ortho*-palladated phenylpyrimidine-1,3-diketonato organyls. In molecules with four or five aliphatic end chains, smectic phases (SmA, SmC) are observed while hexagonal columnar mesomorphism is observed in molecules with seven or eight chains. However, the related compound with six chains in the molecule is non-mesomorphic.

Recently it was observed [54, 57, 58] that the side chain density required for the exhibition of columnar phase was strongly dependent on the size or the flexibility of the core centre, implying that a larger size or a more rigid core requires a larger side chain density. In our case, the crossover of phase change is observed as a function of temperature in a single component with a more rigid core possessing three (single alkyl chain in each ligand) chains at both ends of the molecule, and indeed the alkyl chain density is comparatively lower than the reported compounds. The ionic character of the central core also promotes segregation of

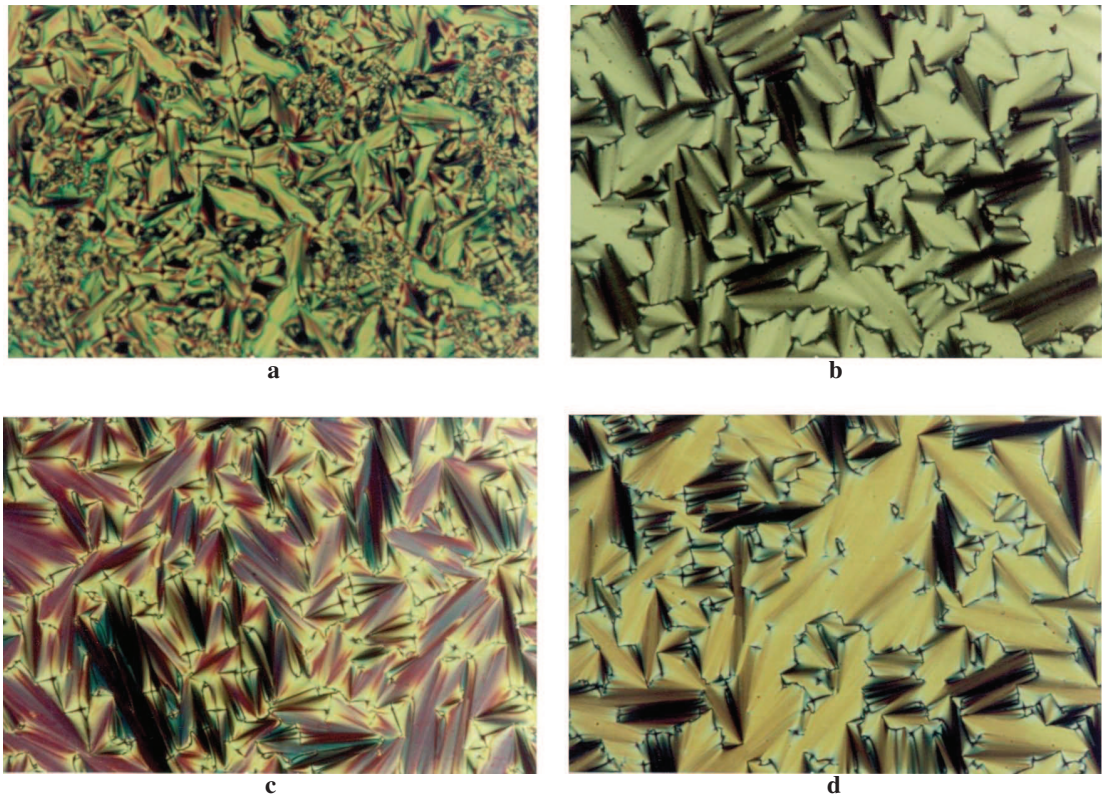

Figure 10. Optical textures exhibited by Dy1, Dy2 and Dy3: (a) focal conic fan texture of SmA exhibited by Dy1 at 145°C; (b) focal conic texture of columnar phase exhibited by Dy2 at 70°C; (c) focal conic fan texture of SmA exhibited by Dy3 at 155°C; and (d) focal conic fan texture of columnar phase exhibited by Dy3 at 130°C (colour version online).

aliphatic chains. The end aliphatic chain contribution is six chains, even though they are of less density in comparison per molecule, but their complexation with a lanthanide metal brings them closer to a cylindrical rod. Moreover, the resulting ionic character from the chemical bonding of the metal-nitro groups and less coordination of metal ion with phenolic groups leads to a distorted ring shape of non uniform diameter at both ends.

3.4 X-ray studies

Three homologues **Tb1, Tb2** and **Tb3** were studied by X-ray diffraction as a function of temperature in different phases with the aim of elucidating the nature of the liquid crystalline phase and determining the lattice parameters. The typical diffractograms obtained for **Tb1, Tb2** and **Tb3** are presented in Figure 12. The largest sharp peak appearing at low angles corresponds to the main periodicity of the system i.e. the layer thickness corresponding to a smectic phase. The low angle spectral pattern was found to be almost identical for the two homologous complexes **Tb2** = 27.7 Å and **Tb3** = 27.7 Å with alkyl chain lengths of 10 and 14 carbons in the aniline moiety and much smaller than the length of the ligands in its fully extended conformation which was evaluated as 35.7 Å for 10O(OH).10 and 40.4 Å for 10O(OH).14.

The temperature variation of layer thickness (Figure 13), also supported the observation of SmA to columnar phase transformation. Furthermore, the layer thickness for the third homologue, **Tb1** = 23.3 Å, is also smaller than the experimental layer thickness of higher homologues and also smaller than the estimated molecular length (28.7 Å) of the coordinating ligand in its fully stretched form. Similar observations of two sharp reflections in the spacing ratio of 1:2 in the small angle region of the X-ray diffraction patterns, inferring smaller layer thickness (31.1 Å) than the estimated molecular length (44.0 Å) for terbium and gadolinium complexes of ligand L7 ($n = 12$, $m = 18$), are reported [20, 29, 33]. The shorter distance of layer thickness than the molecular length has been explained by the interdigitation of aliphatic chains in adjacent layers.

In the present study, however, the homologues **Tb1** in supercooled region, **Tb2** at lower temperature and **Tb3** in the entire temperature range of the mesophase exhibited an X-ray pattern characteristic of hexagonal

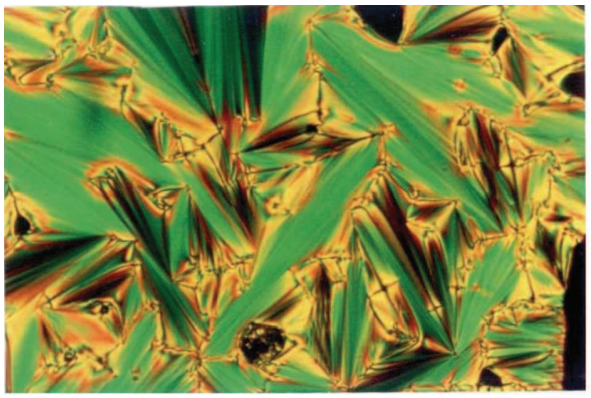

a

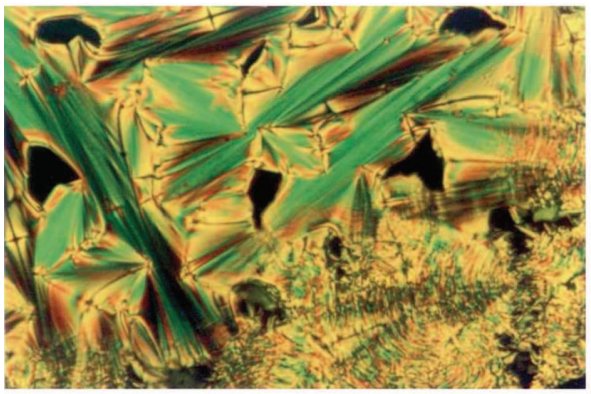

b

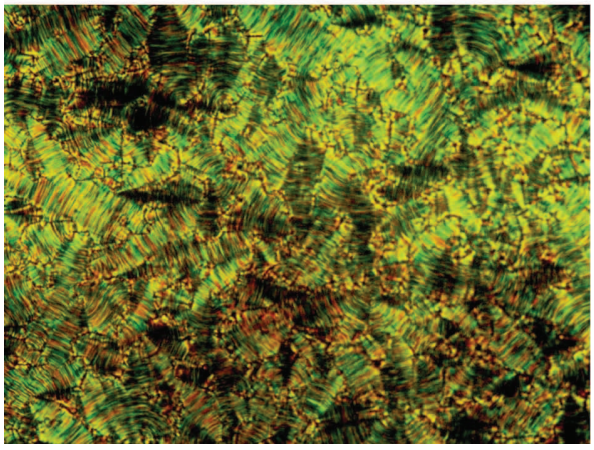

c

Figure 11. Optical textures exhibited by Gd1, Gd2 and Gd3: (a) focal conic fan texture of SmA phase of Gd2 at 157°C; (b) phase transition from SmA to SmE with striations across the fans of Gd2 at 113.5°C; and (c) striations across the fans of SmE phase exhibited by Gd2 at 98°C.

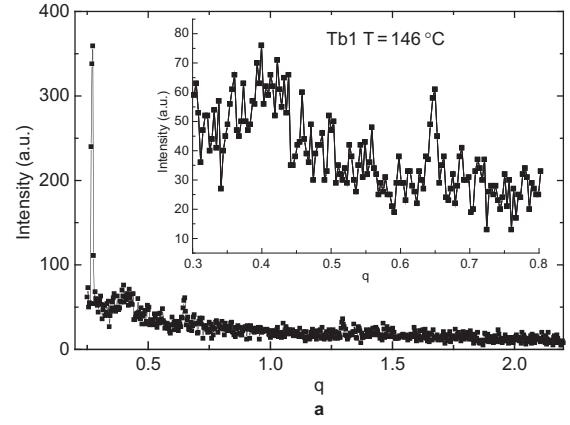

a

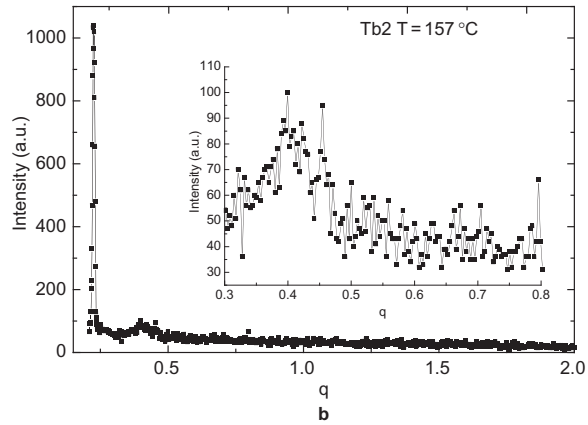

b

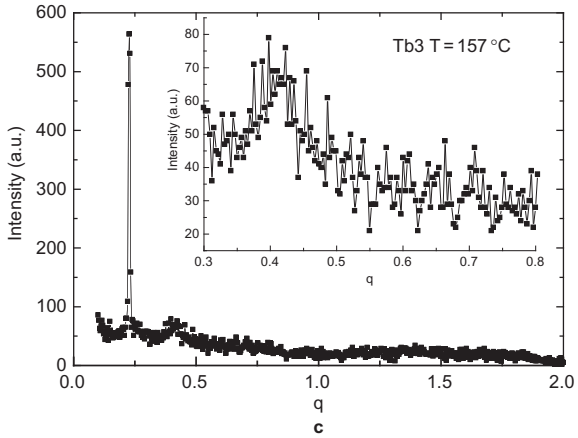

c

Figure 12. X-ray diffractograms of: (a) Tb1 at 148°C; (b) Tb2 at 157°C; and (c) Tb3 at 157°C.

columnar Col_h mesophase (Table 4). The pattern for this phase is characterised by the appearance of a set of three diffraction peaks – a strong peak at 27.7 Å, two weak peaks at a spacing of 15.9 Å and 13.9 Å for **Tb3** – at 165°C in the low angle region with a squared spacing ratio of 1, 3 and 4. These maxima can be assigned to the (10), (11) and (20) reflections from the two-dimensional hexagonal lattice.

Such features are characteristic of a two-dimensional hexagonal packing of columns, suggesting the phase as hexagonal columnar phase (Col_h). The temperature variation of X-ray measurements of **Tb3** did not exhibit any further changes in spectra, reflecting the absence of changes in the molecular structural

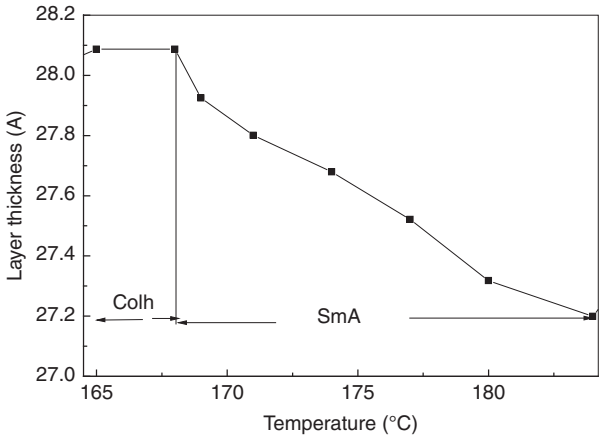

Figure 13. Temperature variation of layer thickness of Tb2.

arrangement in the entire thermal range. In addition to the largest peak in the small angle region, there is a diffuse peak of very low intensity at about 8.9 Å for the terbium complex (X = NO_3).

We believe that the reflections in the 8.0–9.0 Å region correspond to the mean side-to-side distance between the rigid parts of the complexes. A diffuse broad peak of very low intensity was found in the wide angle region, corresponding to the mean distance of 4.3 Å, which is characteristic of liquid crystalline phase. It indicates the liquid-like disorder of the aliphatic alkyl chains as well as the absence of long range periodicity within the columns. As the wide angle scattering is unusually broad in comparison to columnar mesophases of other disc-like compounds, it reflects a strong disorder within the columns.

A possible way to explain the discrepancy between the layer thickness and estimated molecular lengths from the molecular model in its fully extended form in all the cases is as follows. The shorter distance between the smectic layers in comparison to the all *trans* molecular length of the ligand clearly indicate either interdigitation of the aliphatic chains in adjacent layers or confinement within the sublayer by interpenetration of aliphatic chains laterally sideways by spreading in the interfacial region of the layers in the complexes.

In order to control the geometry of the coordination sphere of trivalent lanthanide ion, it is assumed that two nitrate ions are closely occupying the positions in the central core by blocking the four positions of coordination above and below the rare earth cation wrapped by aromatic cores with an extended *N*-aromatic ring of Schiff bases to yield a cylindrical/rod-like object.

Table 4. Characteristic X-ray data of the terbium complexes at different temperatures.

Compound	T (°C)	d_{exp} (Å)	[hk]	I	Mesophase and parameters
Tb1	150	23.3	[10]	VS	SmA
Tb2	174	27.6	[10]	VS	SmA
	157.5	27.9	[10]	VS	Col_h
		15.7	[11]	W	$a = 32.2$ Å
		13.8	[20]	VW	$s = 899$ Å^2
					$V = 2927$ Å^3
					$h = 3.25$ Å
					$N = 1$
Tb3	165	27.7	[10]	VS	Col_h
		15.9	[11]	W	$a = 31.9$ Å
		13.9	[20]	VW	$s = 886$ Å^2
					$V = 3206$ Å^3
					$h = 3.6$ Å
					$N = 1$

Notes: T is the temperature of the XRD experiment, and d_{exp} and d_{calc} are the experimentally measured and calculated diffraction spacings at T, respectively. The distances are given in Å, hk is the indexation of the reflections. Intensity of the reflections: VS = very strong; S = strong; W = weak; VW = very weak; Br = broad (diffuse) reflections, respectively. d_{calc} is deduced from the following mathematical expressions: $<d_{10}> = (1/N_{hk})[\Sigma_{hk} d_{hk}(h^2+k^2+hk)^{1/2}]$ where N_{hk} is the number of hk reflections observed. The lattice parameter 'a' is defined as $a = 2<d_{10}> / \sqrt{3}$ and the lattice area, 'S' is $S = a^2\sqrt{3}/2$. V is the molecular volume and was calculated considering a density of 1g.cm^{-3} according to $V = M/0.6022$, where M is the molecular weight. 'h' is the intracolumnar repeating distance, deduced directly from the calculated molecular volume and the measured columnar cross-section according to $h = NV/S$, where N is the number or a fraction of molecules.

The simple but large electrostatic attraction/repulsion between the rigid cores leading to reduced layer thickness may not explain the mesophase behaviour. The poorly polarisable lipophilic aliphatic chains, which are attached on both sides of the polarisable rigid core, spread over a large area in the interfacial region to complete the rod-like or disc-like molecular structure. Such spreading can also explain the reduced layer thickness.

The incompatibility in space occupation between the polarisable rigid core and poorly polarisable aliphatic continuum organisation and the nature of interfacial curvature between these two incompatible molecular segments define the organisation of molecules in liquid crystalline phase. Hence, the terminal chains occupying the lateral direction increase the microphase segregation effect by enhancing the incompatibility between the rigid cores and flexible aliphatic chains – thereby becoming the driving force for the formation of columnar phases exhibited by the higher homologue as evidenced by the observed textures.

The observation of focal conic fan texture in **Tb2, Dy2** and **Dy3** resembled SmA phase type in the high temperature region and pseudo focal conic fan-like texture resembled the columnar phases in the low temperature region of these compounds. The spread out chains confer a disc-like structure and microscopy confirmed a hexagonal columnar disordered phase. Hence the total diameter of the complex comprising the cation of 2.5 Å and the ligand diameter of 6.0 Å spreading to an average diameter of 8.5–9.0 Å by the complex accounts for the reflection at about 9.0 Å, implying that the complex molecules are arranged side wise in a disc-like fashion.

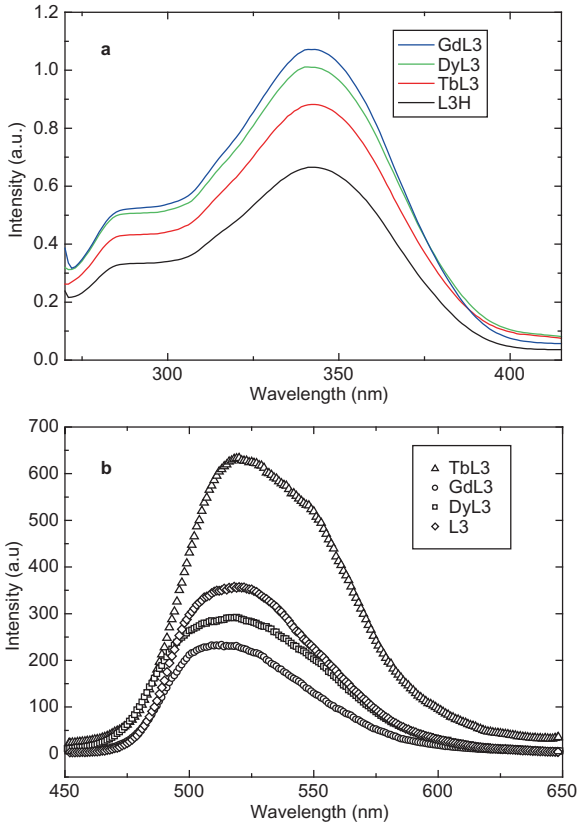

Figure 14. (a) UV-visible optical absorption spectra of ligand L^3H and complexes GdL3, DyL3 and TbL3 recorded in chloroform at the same concentration ($c = 1 \times 10^{-5}$ mol L^{-1}); and (b) emission spectrum of ligand and complexes recorded in chloroform at the same concentration ($c = 1 \times 10^{-5}$ mol L^{-1}).

3.5 Optical absorption and emission studies

The ultraviolet (UV)/visible absorption and fluorescence spectroscopic properties of ligands and complexes in a chloroform solution of different concentrations ($c = 1 \times 10^{-3}$ to 1×10^{-5} mol L^{-1}), (chloroform was chosen as the solvent to maximise molecular solubility) were studied to obtain the information regarding absorption and emission maxima, and the Stokes shift of fluorescence (Figure 14(a)).

The absorption maxima of the lowest optical transition were observed at approximately 340–343 nm for all the ligands and the complexes (~3.6 eV, $\sim\varepsilon$ = 80,000–146,000 mol $L^{-1}.cm^{-1}$), with the other one being at 287 nm (~4.3 eV, 48,000–94,000). The electronic properties of these systems are dominated by the donor–acceptor substituted organic chromophore ligand bands without any noticeable shift to lower or higher energy levels for the complexes, indicating the absence of crystal field effect upon the interelectronic repulsion between the 4f electrons of the metal ion. These absorption bands with large molar absorption coefficients reflect the π–π^* transition of the highly π-conjugated system of the ligand surrounding the metal ion core.

Luminescence studies of metallomesogens are scanty [59] and luminescent studies on the ligand and complexes were carried out in solution and a thin film of the solid phases. The most important features of the photoluminescence emission spectra of the metallomesogens and ligands in chloroform solution at different concentrations and in a thin solid film are the large Stokes shifted emission of ~165–169 nm (Figure 14(b)), and the structureless broad emission band with maxima in the vicinity of ~505 nm.

We did not observe any metal-centred emission and the broad structureless emission band reflects the formation of an intermolecular excimer. The Stokes shift, which reflects the structural relaxation of the

excited molecule, is in the range reported for other metallomesogens [60–62], but significantly larger than the reported push–pull systems [63–67] exhibiting liquid crystal behaviour, confirming the molecular conformational changes upon excitation. Hence it can be assigned to the ligand–ligand charge transfer transition due to the presence of phenyl rings in the ligands and is also indicative of phosphorescence. Further studies are in progress to change the design of the ligand to promote metal-centred absorption and emission.

3.6 Molecular interface and macroscopic organisation and crossover behaviour

The transformation of rod-like to columnar arrangement may be explained as follows. The reduction in size of the metal ion may lead to sterical problems, leading in turn to a less anisotropic complex, while increased charge density of the metal ion leads to a decrease in polarisability which destabilises the SmA phase.

The shape of the molecules, along with their organisation, leads to different mesophases depending on the type of interactions. The density of alkyl chain required to promote the columnar phase is strongly dependent on the size or the flexibility of the central core, i.e. the larger the size or the more rigid is the core group; more side chain density is often needed.

On complexation of three Schiff base units (each have two aliphatic chains) with the lanthanide ion, the side chain density of the system increases to six chains per complex unit (Figure 15) to satisfy the condition to promote the formation of a columnar phase. Further organised arrangement of the alkyl chains of ligands around the central cores of the complex can be explained, in which the Tb(III) ions surrounded by aromatic rings can be visualised as a discoid in shape, with the flexible peripheral aliphatic chains organising themselves either in longitudinal (Figure 15(a), Figure 16(a)) or in lateral (or transverse; Figure 15(b), Figure 16(b)) fashion depending on the density of side chains.

With lesser side chain density, the longitudinal arrangement prevails to exhibit an SmA phase; a larger side chain density prefers the lateral (or transverse) arrangement to exhibit columnar phases. This rearrangement of the side chains allowed the central cores to arrange themselves face-to-face on top of one another forming the columnar phase and the rings containing terbium ions may form chains in the centre of the columns. All this rearrangement duly promoted electrostatic interactions, which are reflected in high melting points.

The number and length of alkyl chains attached to both ends of the molecule, along with extent of spreading of the alkyl chain in the plane of the molecule, plays an important role of interfacial interactions to ensure good compactness between cores and to promote the growth of column [68, 69]. The evaluated intracolumnar distance and surface area, respectively, are h = 3.25 Å, S = 899 Å^2 for **Tb2**, and 3.6 Å and 886 Å^2 **Tb3**. The associated volume of the unit cell can be estimated from $V = S.h$ (2927 Å^3 for **Tb2** and 3206 Å^3 for **Tb3**).

Using the equation $Z = [(d.\mathrm{N_A}.V.10^{-24})/M]$ (d is density, $\mathrm{N_A}$ is Avogadro's number, V is the volume of the unit cell in Å^3 and M is the molecular weight of the molecule in g.mol^{-1}) and assuming the realistic density of these compounds as d $\approx$ 1 g.cm^{-3} in the mesophase, we calculate that the number of molecules per unit cell amounts to $Z = 0.99 \approx 1$ for both compounds **Tb2** and **Tb3**. This strongly suggests that a single complex molecule occupies the cross-section of the column.

The calculated molecular surface area of **Tb2** varied from 107.6 Å^2 at 184°C (below isotropic-SmA transition temperature) to 104.9 Å^2 at 169°C in

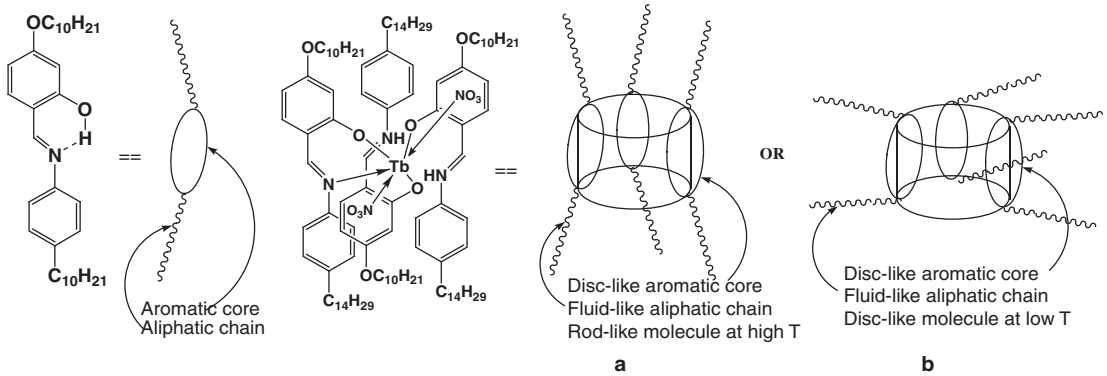

Figure 15. Molecular model of the ligand and complex in: (a) rod-like; and (b) disc-like forms. The coordination of the nitrate ions takes place through the two oxygen atoms of the nitrate ion and, for clarity, the coordination is shown through nitrate ions.

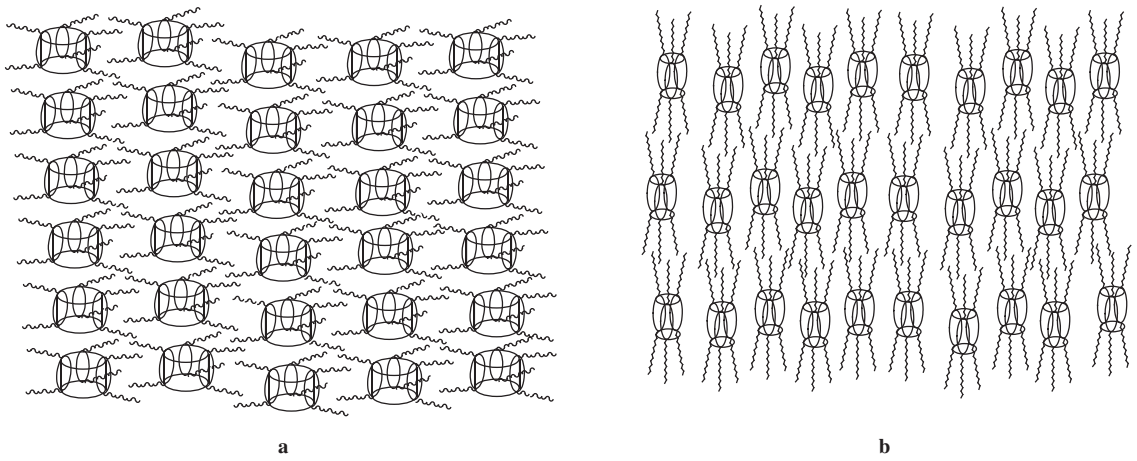

Figure 16. A model for molecular organisations in: (a) columnar; and (b) smectic phases.

SmA phase. The surface area for one Schiff base or azo molecule varies between 30 and 50 $Å^2$ [70–72], and taking into consideration that three Schiff base molecules are embedding the lanthanide ion, the calculated surface area for **Tb2** in SmA phase justifies the large surface area. If the length and number of end chains are less, then they may exhibit rod-like behaviour, i.e. the butyl analogue exhibits a focal conic fan-like texture of the SmA phase of conventional calamitic liquid crystals. When the alkyl chain length is increased to 10 or more carbons to occupy the surrounding space promoting the microphase segregation character, the observed textures are different and resemble the textures characteristic of hexagonal columnar phase observed in compounds exhibiting such phases.

Taking into account of the molecular dimensions obtained from space filling models, as shown in Figure 15(a), (b), the proposed molecular stacking model for the observed SmA and hexagonal columnar phase are shown in Figure 16(a) and (b) respectively. The transformation from lamellar organisation (SmA phase) into a hexagonal columnar arrangement (Col_h) when one additional lateral alkyl chain is connected on the phenyl ring of an aldehyde moiety in lanthanide complexes [29, 50] of ligand **L8** implies the changes in molecular organisation in mesophases. Hence the interactions between the rigid cores and curvature of the interface between incompatible units of the molecule (alkyl chains and rigid core) play an important role in the formation of a particular mesophase. The preliminary results on lanthanide complexes of **L13** in which one of the end alkyl chains in salicylideneimine salicylideneaniline **(L12)** is replaced by a polar group such as F, Cl, CN, NO_2, etc. on an *N*-aryl moiety revealed the absence of columnar phases. Further work is in progress to confirm the transformation in a homologous series by varying the alkyl chains as well as the f-block metal ions.

4. Conclusions

The synthesis of lanthanides complexes of terbium, dysprosium and gadolinium with Schiff bases possessing *N*-aryl groups has been successfully achieved. The enthalpy peaks observed associated with the phase transitions in the first heating cycle of DSC are strongly dependent on the conditions used during the isolation of the virgin compound in the solid state. However, the enthalpy contributions associated with the phase transitions either decrease or disappear in the subsequent cooling and heating cycles, supporting the supercooled glassy state of the mesophase as observed in thermal microscopy. The thermotropic molecules form molecular organisations which divide the space into subspaces and apparently contribute to two distinct micro-domains of aliphatic and aromatic regions depending upon the strength of each of these components and the type of interactions.

It was demonstrated earlier in phasmidic compounds that the core interactions are less important compared with the chemical segregation of aromatic and aliphatic moieties. The resulting mesophases are dependent on the structural arrangement of stacks of molecules whose shape depends on the interface between the semi-rigid core and liquid-like aliphatic chains and not on individual molecules. In the present case, however, the role of the interface between the core and the aliphatic chains in the rod or disc formation is defined by the alkyl chain lengths, which in turn decided the formation of rods or discs on a macroscopic scale to reflect the phase behaviour.

The increased chain length of the terbium compounds leads to only columnar phases. The nature of interactions (Van der Waals interaction, electrostatic interaction) between the lanthanide ion and the coordinating ligand leads to an increase in transition temperatures and thermal stability. Lanthanide complexes exhibit ligand-driven strong fluorescence with a large Stokes shift.

Acknowledgements

Financial assistance is provided by DST, DAE, DRDO and UGC India, International Institute for Complex Adaptive Matter (I2CAM). We are thankful to Professor N.A. Clark and Dr C. Jones for providing X-ray experimental facilities.

References

[1] Serrano, J.L., Ed. *Metallomesogens, Synthesis, Properties and Applications*; VCH: Weinheim, 1996.
[2] Giroud-Godquin, A.M. In *Handbook of Liquid Crystals*: Demus, D., Goodby, J., Gray, G.W., Spiess, H.W., Vill, V., Eds.; Wiley-VCH: Weinheim, 1998; Vol. IIB, pp 901–932.
[3] Giroud-Godquin, A.M.; Maitlis, P.M. *Angew. Chem., Int. Ed. Engl*. **1991**, *30*, 375–402.
[4] Espinet, P.; Esteruelas, M.A.; Oro, L.A.; Serrano, J.L.; Sola, E. *Coord. Chem. Rev*. **1992**, *117*, 215–274.
[5] Bruce, D.W. In *Inorganic Materials*, 2nd ed.; Bruce, D.W., O'Hare, D., Eds.; Wiley: Chichester, 1996; Chapter 8, pp 405–490.
[6] Bruce, D.W. *J. Chem. Soc. Dalton Trans*. **1993**, 2983–2989.
[7] Polishchuk, A.P.; Timofeeva, T.V. *Russ. Chem. Rev*. **1993**, *62*, 291–321.
[8] Hudson, S.A.; Maitlis, P.M. *Chem. Rev.* **1993**, *93*, 861–865.
[9] Oriol, L.; Serrano, J.L. *Adv. Mater*. **1995**, *7*, 348–369.
[10] Hoshino, N. *Coord. Chem. Rev*. **1998**, *174*, 77–108.
[11] Donnio, B.; Bruce, D.W. *Struct. Bond.* **1999**, *95*, 193–247.
[12] Donnio, B.; Guillon, D.; Deschenaux, R.; Bruce, D.W. In *Comprehensive Coordination Chemistry II: From Biology to Nanotechnology*; McCleverty, J.A., Meyer, T.J., Eds.; Elsevier: Oxford, 2003; *7*, pp 357–627.
[13] Bruce, D.W.; Deschenaux, R.; Donnio, B.; Guillon, D. In *Comprehensive Organometallic Chemistry III*; Crabtree, R.H., Mingos, D.M.P., Eds.; Elsevier: Oxford, UK, 2007; Vol. 12, Chapter 12.05, pp 195–293.
[14] Galyametdinov, Y.G.; Ivanova, G.I.; Ovchinnikov, I.V. *Bull. Acad. Sci. USSR Div. Chem. Sci*. **1991**, *40*, 1109.
[15] Terazzi, E.; Suarez, S.; Torelli, S.; Nozary, H.; Imbert, D.; Mamula, O.; Rivera, J.P.; Guillet, E.; Benech, J.M.; Bernardinelli, G.; Scopelliti, R.; Donnio, B.; Guillon, D.; Bunzli, J.C.G.; Piguet, C. *Adv. Funct. Mater*. **2006**, *16*, 157–168.
[16] Piguet, C.; Bunzli, J.C.G. *Chem. Soc. Rev.* **1999**, *28*, 347–358.
[17] Bunzli, J.C.G. *Acc. Chem. Res.* **2006**, *39*, 53–61.
[18] Bunzli, J.C.G.; Piguet, C. *Chem. Rev.* **2002**, *102*, 1897–1928; *Chem. Soc. Rev.* **2005**, *34*, 1048–1077.
[19] Terazzi, E.; Torelli, S.; Bernardinelli, G.; Rivera, J.P.; Benech, J.M.; Bourgogne, C.; Donnio, B.; Guillon, D.; Imbert, D.; Bunzli, J.C.G.; Pinto, A.; Jeannerat, D.; Piguet, C. *J. Am. Chem. Soc.* **2005**, *127*, 888–903.
[20] Binnemans, K.; Gorller-Walrand, C. *Chem. Rev*. **2002**, *102*, 2303–2345.
[21] Binnemans, K.; Galyametdinov, Yu.G.; Van Deun, R.; Bruce, D.W.; Collinson, S.R.; Polishchuk, A.P.; Bikchantaev, I.; Haase, W.; Prosvirin, A.V.; Tinchurina, L.; Litvinov, I.; Gubajdullin, A.; Rakhmatullin, A.; Uytterhoeven, K.; Van Meervelt, L. *J. Am. Chem. Soc*. **2000**, *122*, 4335–4344.
[22] Galyametdinov, Yu.G.; Ivanova, G.I.; Prosvirin, A.V.; Kadkin, O. *Russ. Chem. Bull*. **1994**, *43*, 938–940.
[23] Van Deun, R.; Binnemans, K. *Liq. Cryst*. **2001**, *28*, 621–627; *Mater. Sci. Eng. C*. **2001**, *18*, 211–215.
[24] Binnemans, K.; Van Deun, R.; Gorller-Walrand, C.; Haase, W.; Bruce, D.W.; Malykhina, L.; Galyametdinov, Yu.G. *Mater. Sci. Eng. C*. **2001**, *18*, 247–254.
[25] Galyametdinov, Yu.G.; Haase, W.; Malykhina, L.; Prosvirin, A.; Bikchantaev, I.; Rakmatullin, A.; Binnemans, K. *Chem. Eur. J*. **2001**, *7*, 99–105.
[26] Binnemans, K.; Moors, D.; Parac-Vogt, T.N.; van Deun, R.; Hinz, H.; Meyer, G. *Liq. Cryst*. **2002**, *29*, 1209–1216.
[27] Van Deun, R.; Binnemans, K. *J. Alloys Comp*. **2000**, *303–304*, 146–150.
[28] Binnemans, K.; Lodewyckx, K.; Van Deun, R.; Galyametdinov, Yu.G.; Hinz, D.; Meyer, G. *Liq. Cryst*. **2001**, *28*, 279–285.
[29] Galyametdinov, Yu.G.; Athanassopoulou, M.A.; Griesar, K.; Kharitonova, O.; Soto Bustamante, E.A.; Tinchurina, L.; Ovchinnikov, I.; Haase, W. *Chem. Mater.* **1996**, *8*, 922–926.
[30] Binnemans, K.; Galyametdinov, Yu.G.; Collinson, S.R.; Bruce, D.W. *J. Mater. Chem*. **1998**, *8*, 1551–1553.
[31] Binnemans, K.; Van Deun, R.; Bruce, D.W.; Galyametdinov, Yu.G. *Chem. Phys. Lett*. **1999**, *300*, 509–514.
[32] Martin, F.; Collinson, S.R.; Bruce, D.W. *Liq. Cryst*. **2000**, *27*, 859–863.
[33] Galyametdinov, Yu.G.; Ivanova, G.; Ovchinnikov, I.; Prosvirin, A.; Guillon, D.; Heinrich, B.; Dunmur, D.A.; Bruce, D.W. *Liq. Cryst*. **1996**, *20*, 831–833.
[34] Turanov, A.N.; Ovchinnikov, I.V.; Galyametdinov, Yu.G.; Ivanova, G.I.; Goncharov, V.A. *Russ. Chem. Bull*. **1999**, *48*, 690–693.
[35] Galyametdinov, Yu.G.; Ivanova, G.I.; Ovchinnikov, I.V.; Binnemans, K.; Bruce, D.W. *Russ. Chem. Bull.* **1999**, *48*, 385–387.
[36] Galyametdinov, Yu.G.; Atanassopoulo, M.; Khaaze, V.; Ovchinnikov, I.V. *Russ. J. Coord. Chem.* **1995**, *21*, 718–719.
[37] Yelamaggad, C.V; Prabhu, R.; Shanker, G.; Bruce, D.W. *Liq. Cryst*. **2009**, *36*, 247–255.
[38] Bellusci, A.; Barberio, G.; Crispini, A.; Ghedini, M.; La Deda, M.; Pucci, D. *Inorg. Chem.* **2005**, *44*, 1818–1825.
[39] Cardinaels, T.; Driesen, K.; Parac-Vogt, I.N.; Heinrich, B.; Bourgogne, C.; Guillon, D.; Donnio, B.; Binnemans, K. *Chem. Mater*. **2005**, *17*, 6589–6598.

[40] Nozary, H.; Piguet, C.; Tissot, P.; Bernardinelli, G.; Bunzli, J.C.G.; Deschenaux, R.; Guillon, D. *J. Am. Chem. Soc*. **1998**, *120*, 12274–12288.
[41] Nozary, H.; Piguet, C.; Rivera, J.P.; Tissot, P.; Bernardinelli, G.; Vulliermet, N.; Weber, J.; Bunzli, J.C.G. *Inorg. Chem*, **2000**, *39*, 5286–5298.
[42] Nozary, H.; Piguet, C.; Rivera, J.P.; Tissot, P.; Morgantini, P.Y.; Weber, J.; Bernardinelli, G.; Bunzli, J.C.G.; Deschenaux, R.; Donnio, B.; Guillon, D. *Chem. Mater.* **2002**, *14*, 1075–1090.
[43] Terazzi, E.; Benech, J.M.; Torelli, S.; Rivera, J.P.; Bernardinelli, G.; Donnio, B.; Guillon, D.; Piguet, C. *J. Chem. Soc. Dalton Trans.* **2003**, 769–772.
[44] Piguet, C.; Bunzli, J.C.G.; Donnio, B.; Guillon, D. *Chem. Comm.* **2006**, 3755–3768.
[45] Terazzi, E.; Guenee, L.; Morgantini, P.Y.; Bernardinelli, G.; Donnio, B.; Guillon, D.; Piguet, C. *Chem. Eur. J.* **2007**, *13*, 1674–1691.
[46] Nozary, H.; Torelli, S.; Guenee, L.; Terazzi, E.; Bernardinelli, G.; Donnio, B.; Guillon, D.; Piguet, C. *Inorg. Chem.* **2006**, *45*, 2989–3003.
[47] Binnemans, K.; Bruce, D.W.; Collinson, S.R.; Van Deun, R.; Galyametdinov, Yu.G.; Martin, F. *Phil. Trans. R. Soc. Lond. A* **1999**, *357*, 3063–3077.
[48] Binnemans, K. *Mat. Sci. Forum* **1999**, *315*, 169–174.
[49] Rao, N.V.S.; Paul, M.K.; Rao, T.R.; Prasad, A. *Liq. Cryst.* **2002**, *29*, 1243–1246.
[50] Rao, N.V.S.; Choudhury, T.D.; Paul, M.K.; Francis, T. *Liq. Cryst.* **2009**, *36*, 409–423.
[51] Alapati, P.R.; Rao, P.B.; Rao, N.V.S.; Pisipati, V.G.K.M. *Mol. Cryst. Liq. Cryst. Lett.* **1988**, *5*, 73–78.
[52] Gray, G.W.; Goodby, J.W. *Smectic Liquid Crystals: Textures and Structures*; Heyden & Son: Philadelphia, 1984.
[53] Elliot, J.M.; Chipperfield, J.R.; Clark, S.; Sinn, E. *Inorg. Chem. Commun*. **2002**, *5*, 99–101.
[54] Elliot, J.M.; Chipperfield, J.R.; Clark, S.; Sinn, E. *Inorg. Chem*. **2001**, *40*, 6390–6396.
[55] Collinson, S.R.; Martin, F.; Binnemans, K.; Van Deun, R.; Bruce, D.W. *Mol. Cryst. Liq. Cryst*. **2001**, *364*, 745–752.
[56] Hegmann, T.; Peidis, F.; Diele, S.; Tschierske, C. *Liq. Cryst.* **2001**, *27*, 1261–1265.
[57] Majumdar, K.C.; Pal, N.; Debnath, P.; Rao, N.V.S. *Tetrahedron Lett*. **2007**, *48*, 6330–6333.
[58] Wang, Y.J.; Sheu, H.S.; Lai, C.K. *Tetrahedron* **2007**, *63*, 1695–1705.
[59] Binnemans, K. *J. Mater. Chem*. **2009**, *19*, 448–453.
[60] Pucci, D.; Barberio, G.; Bellusci, A.; Crispini, A.; Donnio, B.; Giorgini, L.; Ghedini, M.; Deda, M.L.; Szerb, E.I. *Chem. Eur. J.* **2006**, *12*, 6738–6747.
[61] Bayon, R.; Coco, S.; Espinet, P. *Chem. Eur. J.* **2005**, *11*, 1079–1085.
[62] Arias, J.; Bardaji, M.; Espinet, P. *Inorg. Chem.* **2008**, *47*, 3559–3567.
[63] Gallardo, H.; Cristiano, R.; Vieira, A.A.; Neves Filho, R.A.W.; Srivastava, R.M.; Bechtold, I.H.; *Liq. Cryst*. **2008**, *35*, 857–863.
[64] Vieira, A.A.; Cristiano, R.; Bortoluzzi, A.J.; Gallardo, H. *J. Mol. Struct.* **2008**, *875*, 364–371.
[65] Srivastava, R.M.; Neves Filho, R.A.W.; Schneider, R.; Vieira, A.A.; Gallardo, H. *Liq. Cryst.* **2008**, *35*, 737–742.
[66] Cristiano, R.; Ely, F.; Gallardo, H. *Liq. Cryst*. **2005**, *32*, 15–25.
[67] Vieira, A.A.; Cristiano, R.; Ely, F.; Gallardo, H. *Liq. Cryst*. **2006**, *33*, 381–390.
[68] Chandrasekhar, S. In *Handbook of Liquid Crystals*: Demus, D., Goodby, J., Gray, G.W., Spiess, H.W., Vill, V., Eds.; Wiley-VCH: Weinheim, 1998; Vol. IIB, pp 749–780.
[69] Nguyen, H.T.; Destrade, C.; Malthete, J. In *Handbook of Liquid Crystals*: Demus, D., Goodby, J., Gray, G.W., Spiess, H.W., Vill, V., Eds.; Wiley-VCH: Weinheim, 1998; Vol. IIB, pp 865–885.
[70] Guillon, D.; Mathis, A.; Skoulios, A. *J. Physique* **1975**, *36*, 695–700.
[71] Albertini, G.; Fanelli, E.; Guillon, D.; Melone, S.; Poeti, G.; Rustichelli, F.; Torquati, G. *J. Chem. Phys*. **1983**, *78*, 2013–2016.
[72] Albertini, G.; Fanelli, E.; Guillon, D.; Melone, S.; Poeti, G.; Rustichelli, F.; Torquati, G. *J. Physique* **1984**, *45*, 341–346.